Eur. Phys. J. B **30**, 393–398 (2002)
DOI: 10.1140/epjb/e2002-00394-3

THE EUROPEAN PHYSICAL JOURNAL B

SnO_2 quantum dots confined in a glass matrix

G. Faraci[1,a], A.R. Pennisi[1], and A. Balerna[2]

[1] Dipartimento di Fisica e Astronomia, Universitá di Catania, Istituto Nazionale di Fisica della Materia, Corso Italia 57, 95129 Catania, Italy
[2] Istituto Nazionale di Fisica Nucleare, Laboratori Nazionali di Frascati, 00044 Frascati, Italy

Received 6 May 2002 / Received in final form 11 October 2002
Published online 19 December 2002 –

Abstract. We report on the formation and detection of SnO_2 quantum dots confined in a glass matrix. The average radius of these agglomerates embedded in a B_2O_3 substrate was evaluated in 5, 10, and 14 Å for a 0.1, 0.2, and 0.3% dilution of the semiconductor in the glass, respectively. The characterization of the samples was performed by EXAFS (Extended X-ray Absorpion Fine Structure) and XRD (X-ray diffraction) spectroscopies.

PACS. 61.46.+w Nanoscale materials: clusters, nanoparticles, nanotubes, and nanocrystals – 61.10.-i X-ray diffraction and scattering – 81.07.Ta Quantum dots

1 Introduction

High gap semiconductors such as SnO_2 [1–3], In_2O_3 [4], $SnInO_x$ (ITO) [5], are a class of oxides which exhibit high optical transparency and good electrical conductivity; when doped or mixed with a metal (*e.g.*, Sn doped In_2O_3), or a semiconductor (*e.g.*, $Ga_{3-x}In_{5+x}Sn_2O_{16}$) [6], they assume a higher conductivity maintaining a good transparency. Therefore, these transparent conducting oxides find large applications in several devices, in the field of optoelectronics and microelectronics as thin films or nanostructures, as well as gas sensors [7].

The properties of these oxides can be largely dependent on their geometrical characteristics such as film thickness and surface roughness [5], crystalline or amorphous phase [1], grain size and porosity [1–3]. Of course, important modifications can be caused by doping centers [8,9]. Also size confinement, involving small clusters or quantum dots of these oxides [2,8,10], represents a bright expedient for obtaining novel challenging properties in material science. In fact, quantum size effects can dramatically modify the energy level distribution both in the valence and in the conduction bands [11], with the possibility to build up optical transitions shifted or modified according to the particular technological application. For this reason the present study concerns the confinement of SnO_2 quantum dots.

In principle, it is necessary to realize a high concentration of dots with proper size in a suitable matrix; this is however not an easy task for several reasons: the first is related to the difficulties of obtaining size selected clusters; the second is due to the choice of the matrix, or of a proper solution which should prevent any possible influence of the solvent on the properties of the solute; and finally, the finding of a suitable experimental procedure, including the eventual thermal treatment, for obtaining the precipitation of size selected quantum dots with reduced dispersion.

With reference to matrix-induced effects, it is worth to point out the interface properties due to bonds of the confined clusters with the host material; internal volume and surface layer of the clusters can have a quite different behaviour, with a relative weight, size and shape dependent. In addition, care should be paid in melting procedures and in solid solutions about possible mixing of elements of the matrix with those of the solute [4]. In a previous paper [4] in fact, we obtained an experimental sintering of indium borate clusters by simple melting of indium oxide in a boron oxide matrix. We adopted the same procedure to obtain precipitates of SnO_2 quantum dots in a glass matrix (B_2O_3), avoiding however any chemical modification of the solute. This goal was achieved because tetravalent tin cannot be substituted by trivalent boron in a SnO_2 configuration, and this prevents the formation of tin and boron mixed oxide; however, two tin oxides are most common, namely SnO and SnO_2 [12]. Fortunately, these oxides present quite different geometrical configuration: in fact, stannous oxide (SnO) is tetragonal with $a = 3.802$ and $c = 4.836$, whereas stannic oxide (SnO_2) crystallizes in the cassiterite structure (space group p42/mnm) with octahedral coordination and tetragonal symmetry having $a = 4.73727$, $c = 3.186383$ and $u = 0.307$ [13]. The remarkable difference in the lattice parameters, and precise X-ray diffraction characterization of the samples have excluded any presence of foreign

[a] e-mail: Giuseppe.Faraci@ct.infn.it

oxides different from the wanted semiconductor. In order to fully characterize the quantum dots precipitated in the matrix we adopted the Extended X-ray Absorption Fine Structure (EXAFS) spectroscopy. In fact, this technique allows the investigation of the geometrical configuration around the absorbing Sn atom, permitting to distinguish between oxygen and tin coordination; moreover, this spectroscopy is a short range probe permitting the determination of the mutual distances and coordination numbers related to some coordination shells around the central atom; finally, also the vibrational and thermodynamical parameters (Debye-Waller factor and Debye temperature) can be obtained by these measurements, acquiring some insight in the interface configuration related to the phonon coupling with the matrix [14–16]. In the following we report about a simple melting procedure producing SnO_2 quantum dots, whose size can be selected by just choosing the appropriate dilution; at very low concentration (0.05%) the separation between the solute molecules is so large that only the first Sn-O coordination is visible but with lower coordination numbers, with respect to the crystal. This corresponds to single molecular aggregates embedded into the matrix.

2 Experiment

In order to obtain nanocrystals of SnO_2 in the B_2O_3 matrix we used, as already mentioned, the same melting procedure detailed in reference [4], mixing with the matrix high purity SnO_2 at the desired concentration; a wide temperature range was explored between 1000 °C and the melting temperature of the solute (1625 °C) quite higher than the melting point of the matrix (450 °C). Some samples were checked by XRD, together with the pure constituents. In Figure 1 typical XRD spectra are reported: the peaks of the SnO_2 crystal are well reproduced in the diluted sample where also the B_2O_3 features are present; in general, as expected, the high concentration solid solutions presented the same features of the constituents, although, of course, with reduced intensity of the solute. The low dilution samples, on the contrary, showed only qualitative modifications quantitatively investigated afterwards by EXAFS spectroscopy.

The EXAFS experiment was performed at the GILDA beamline [17,18] of the European Synchrotron Radiation Facility (ESRF, Grenoble, France); the radiation was monochromatised and horizontally focused by a crystal Si(311) monochromator. The beam spot on the sample was 1×2 mm^2; the energy resolution was in the order of 10^{-5}. X-ray spectra were collected around the Sn K-edge (29 200 eV). The measurements were performed at 77 K, in fluorescence, using an ultrapure 13-element Ge multidetector cooled at 77 K, but also the absorption detection was adopted for high concentration (0.4–5.%) samples, considering the very low absorbance of the matrix. For reference, a thin layer of SnO_2 powder polycrystal was used, together with a high purity Sn foil in order to get the experimental Sn-Sn phases.

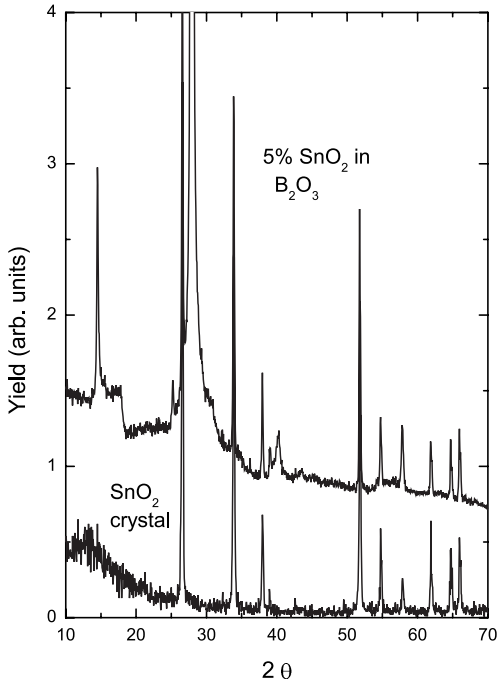

Fig. 1. Lower curve: XRD spectrum of the SnO_2 crystal as a function of the diffraction angle 2θ; upper curve: XRD spectrum for the diluted 5% sample; here, the extra peaks are due to the glass matrix.

We recall first, the composition of the semiconductor and its geometrical configuration around a Sn absorber [13]. A distorted octahedral distribution of oxygen atoms surrounds the Sn central atom, with 4 O at 2.05186 Å and other 2 O at 2.05675 Å; considering the quite small difference between the distances of these oxygen atoms, and taking into account that the EXAFS accuracy for interatomic distances is, in our case, of about 0.01 Å we can treat the six oxygen atoms as forming a single first shell. In the second coordination shell, 2 Sn atoms reside at 3.18638 Å whereas in the third one we find 4 O atoms at 3.59064; in the fourth shell 8 Sn atoms are at 3.70933 Å. These values are also reported in Table 1 as diffraction data, directly verified for the pure dioxide by XRD. No evidence was found of SnO whose composition we report here only for the sake of clarity: first, second, third, and fourth shell is respectively formed by 4 O (at 2.227 Å), 4 Sn (3.5519 Å), 4 Sn (3.6812 Å), 4 Sn (3.8020 Å). The distances are so different with respect to SnO_2 that no ambiguity can occur.

The normalized EXAFS spectra were analysed according to a standard procedure [14,15,21,22] removing the background by means of a cubic spline and fitting the continuous component of the spectrum in the k range. From the raw curves, after normalization and subtraction of the background we can extract the EXAFS oscillations $\chi(k)$. These curves, weighted by k^2, or k^3, have been Fourier transformed in the range $\Delta k = 2.5{-}19.6$ Å^{-1}. Their peaks correspond to the first and successive coordination shells due to the local average configuration of each sample.

Table 1. Parameters of the first, second, and fourth shells around an Sn absorber for our diluted samples, obtained by the FEFFIT code applied to the FTs of the EXAFS spectra; here, the uncertainty for the coordination numbers is ±0.1 and for the lowest dilution ±0.2; for all the fitted distances the uncertainty is ±0.01 Å, for the DW factors ±0.0004 Å^2.

dilution	first shell: Sn-O			second shell: Sn-Sn			fourth shell: Sn-Sn		
(%)	N	R (Å)	$\sigma^2(\times10^{-4}$ Å$^2)$	N	R (Å)	$\sigma^2(\times10^{-4}$ Å$^2)$	N	R (Å)	$\sigma^2(\times10^{-4}$ Å$^2)$
0.05	5.3	2.01	57.0	–	–	–	–	–	–
0.1	4.3	2.01	54.0	0.75	3.18	43.0	4.1	3.71	41.0
0.2	4.8	2.035	50.0	1.5	3.18	19.0	5.8	3.72	18.0
0.3	5.3	2.05	26.0	1.65	3.18	16.0	6.5	3.715	18.0
0.5	6.0	2.05	18.0	2.0	3.19	7.0	8.0	3.715	17.0
5.0	6.0	2.055	10.0	2.0	3.19	7.0	8.0	3.71	11.0
crystal	6.0	2.054	16.0	2.0	3.19	12.0	8.0	3.71	17.0

3 Results and discussion

Firstly, in Figure 2 we display the raw absorption spectrum for the reference SnO_2 thin layer together with the $k\chi(k)$ EXAFS spectrum and the FT of the $k^3\chi(k)$. This spectrum shows the first peak due to the oxygen first shell around the absorbers, and two adjacent peaks to be ascribed to Sn second and fourth coordination shells (see Tab. 1), with a negligible contribution of the third oxygen shell. The two metal peaks appear so well separated for two reasons: i) the first, clearly, has to be attributed to the low temperature of the experiment (77 K); ii) the second, to the excellent resolution permitted by the persistence of the EXAFS oscillations up to high k values; note, in addition, that the weighting factor, in the Fourier transform of $k^3\chi(k)$, strongly reduces the influence of higher oxygen shells with respect to the contribution of a heavy metal like Sn. Actually, the oxygen third shell with 4 O at 3.59 Å, falling between the two Sn peaks, has a very reduced intensity as afterwards evaluated during the fitting procedure. The verification of the proper parameters for each shell was performed applying to the $k^n\chi(k)$ $(n = 2, 3)$ curve and to its FT an accurate fitting code (FEFF) using curved wave calculations, multiple scattering paths and inelastic losses [21,22]. As reported in Table 1, the fit permitted the determination of the main parameters (coordination number N, interatomic distance R, Debye-Waller factor σ^2), together with other important factors such as the attenuation factor S_0^2 (due to shake-up and shake-off contributions), the cumulants corrections etc. In particular, we first fitted the parameters of the reference crystal reported in Table 1; no constraint was used; an excellent agreement can be observed in Figure 2 between the experimental FT of the reference compound and the best fit curve obtained with the corresponding parameters of Table 1.

This fit permitted the determination of the overall S_0^2 amplitude factor [14,15] ($S_0^2 = 0.95$) which was fixed in the diluted samples analysis.

It is worth to point out that we performed a more detailed analysis introducing the cumulants in the fit, in order to check whether the distance distribution was somewhat distorted; as expected, only the fourth cumulant for the oxygen first shell was found quite small (of the order of 10^{-5}), whereas the others were zero.

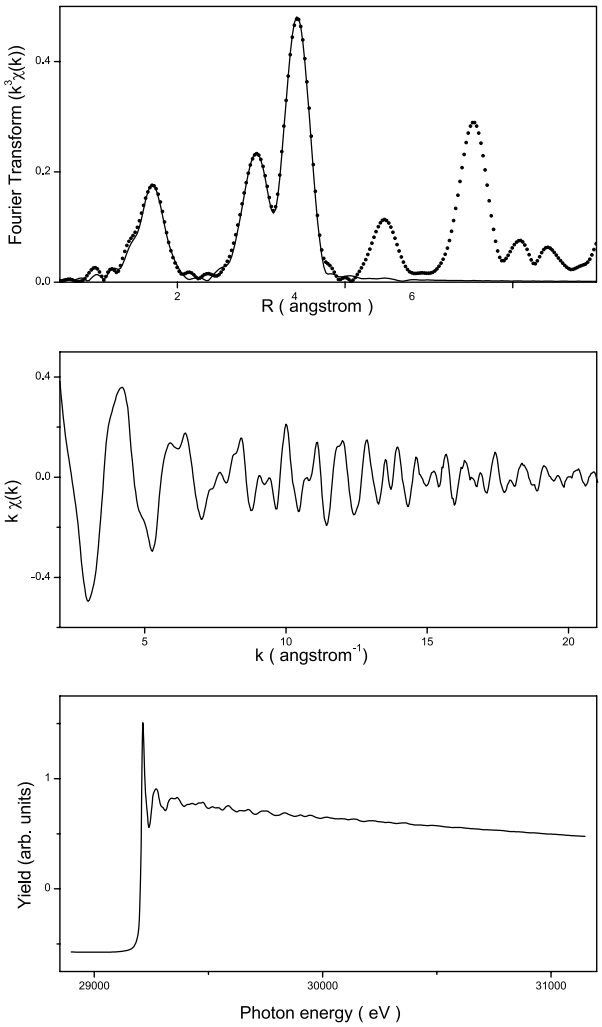

Fig. 2. Lower curve: absorption spectrum as a function of the photon energy for the reference SnO_2 crystal; middle curve: k weighted EXAFS oscillations of the reference sample, as a function of the wave vector k, extracted from the raw spectrum after normalization and background subtraction; upper curve: FT of the k^3 weighted $\chi(k)$, together with the fitting curve (continuous line) of the first three peaks, using the FEFFIT code. The correspondent parameters are reported in Table 1. The fitted peaks are due to the first, second and fourth shells. Also visible two other features mainly arising from metal higher shells which were not fitted.

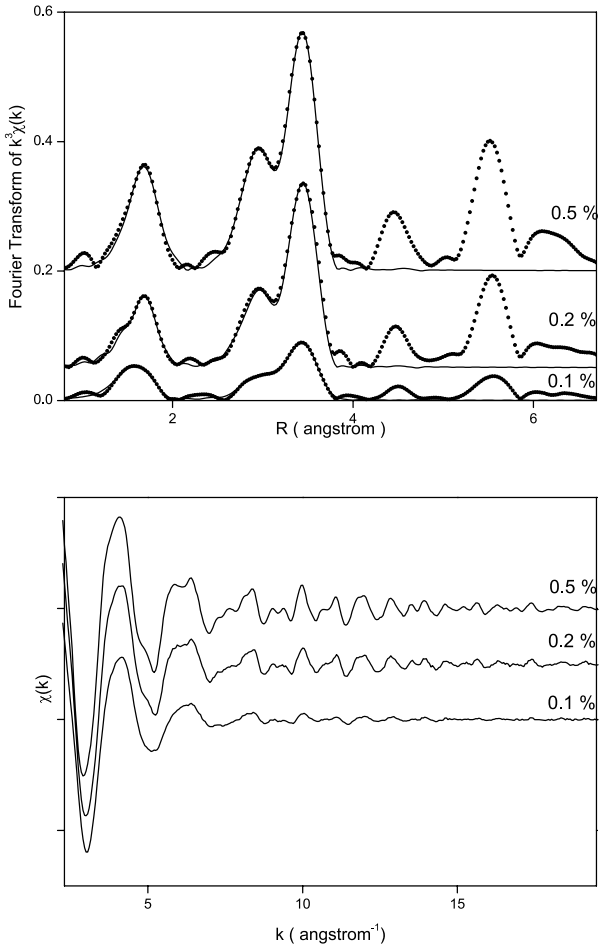

Fig. 3. Lower curves: typical EXAFS oscillations for some dilutions of SnO_2 in a B_2O_3 matrix, as a function of the wave vector k, extracted from the raw spectra after normalization and background subtraction; upper curves: FT of the k^3 weighted $\chi(k)$, together with the fitting curve (continuous line) of the first three peaks, using the FEFFIT code. The correspondent parameters are reported in Table 1. The fitted peaks are due to the first, second and fourth shells. Also visible two other features arising mainly from metal higher shells which were not fitted. The curves were shifted for the sake of clarity.

Although the FT of Figure 2 shows evident higher shell peaks beyond 4 Å, these were not fitted, because, at higher distances, several contributions overlap, due to metal and oxygen higher shells, mixed up with multiple (three or more paths) scatterings; therefore, the reliability of too many parameters is quite uncertain even though the oxygen contribution as already mentioned is strongly damped; in fact, we evaluated that in the curve of the FT (Fig. 2) the third O shell at 3.59 Å has a relative yield lower than 6% and for this reason it was neglected [23].

In Figure 3 we can now display some typical EXAFS spectra for several dilutions; in these measurements, in order to improve the statistical accuracy, many spectra were collected for each experimental configuration, and, as reported elsewhere [15], an accurate statistical analysis was always performed within the fitting procedure by the minimization of the reduced χ^2.

In the same Figure 3 we also show the FT of the $k^3\chi(k)$ and the best fit obtained by the same procedure and in the same conditions as for the reference compound. The correspondent parameters are inserted in Table 1.

We observe: i) at concentration higher than 0.5%, the coordination numbers for the first oxygen shell as well as for the Sn-Sn successive shells are identical to those of the crystal; also the distances are finely reproduced, well within the accuracy of the EXAFS technique (0.01 Å). The mean-squared relative displacement σ^2 can also be considered without severe changes.

In contrast, at concentration lower than 0.5%, as visible in Table 1, all the parameters undergo a dramatic modification. In fact, all the samples investigated from 0.5 to 0.1% show a progressive reduction of the coordination numbers of the first oxygen shell as well as of the second and of the fourth metal shell. In concomitance, we observe a very small contraction of the distance Sn-O but the metal-metal mutual position does not change at all; instead, the Debye-Waller factor uniformly increases for all the shells; as far as concerns the cumulants, we find a small contribution only in the first shell ($C_4 = -2.0 \times 10^{-5}$ Å^4) taking into account the weak asymmetry of this peak. Finally, at the lowest 0.05% dilution (so low that its uncertainty is about $\pm 0.03\%$, with a lower signal-to-noise ratio) the χ spectrum and the $k\chi(k)$ FT show respectively a single frequency and a single peak corresponding only to the Sn-O coordination (see Fig. 4 and Tab. 1). In all the cases reported in the table, also the correlation between N and σ^2 was accurately checked together with their influence on the error bars: as visible in the table, the samples at highest dilutions are in fine agreement with the reference crystal, whereas the lower dilution (0.1–0.3%) samples show a regular trend for all the three parameters reported for each shell.

Discussing in more details the previous results we emphasize, first of all, the important result obtained at 0.05%. This concentration shows that the melting process, at least in the present matrix, is able to completely separate the tin dioxide molecules in the single molecular constituents; this conclusion, supported by the absence of any metal-metal peak in the FT, indicates an uniform distribution in the B_2O_3 matrix of SnO_x molecules quite distant from each other, in which the metal can be sometimes in substoichiometric configuration; in fact, a first coordination number equal to 6 oxygen atoms would mean an exact stoichiometric distribution of SnO_2 molecules if a non local distribution of metal atoms would maintain the correct ratio 1:2 between the number of metal atoms and the number of oxygen atoms; when single tetravalent Sn atoms are locally confined and still most of the original SnO_6 octahedra survive (very likely mixed with SnO_4 aggregates) this implies that the oxygen atoms should bind not only tin but also the matrix constituents. In this case, a coordination 5.3 could result as the average of 65% and 35% of SnO_6 and SnO_4 aggregates, respectively; this is corroborated by the somewhat contracted distance owed to the absence of further oxygen-metal bonds, by the increase of the DW factor, and by the fourth cumulant

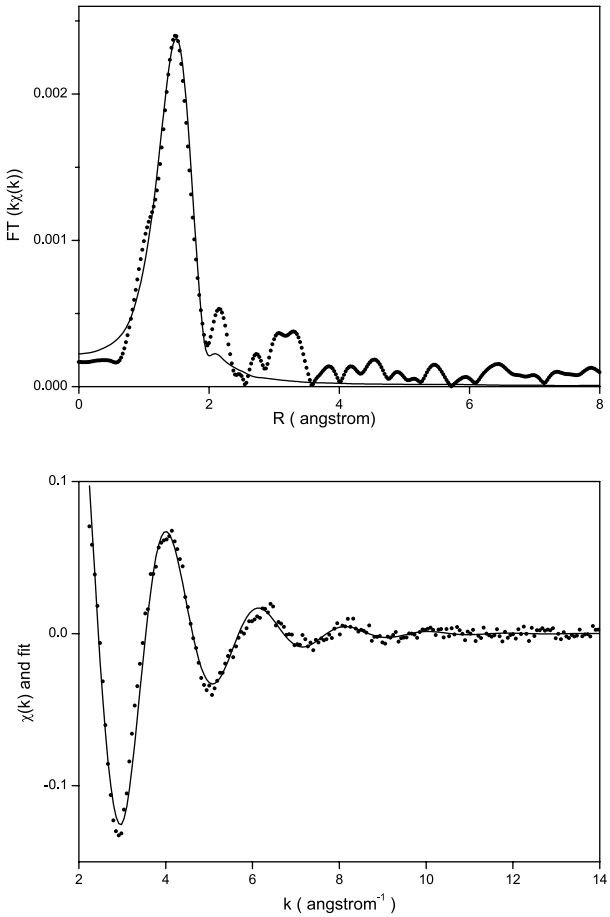

Fig. 4. 0.05% dilution. Lower curve: EXAFS oscillations as a function of the wave vector k, extracted from the raw spectrum after normalization and background subtraction. Also reported the fitting curve using the FEFFIT code; upper curve: FT of the k weighted $\chi(k)$, together with the fitting curve (continuous line) of the first peak, using the FEFFIT code. This peak is due to the oxygen coordination shell around the Sn absorber. No other feature is clearly visible out of the noise level at the lowest dilution. The correspondent parameters are reported in Table 1.

$C_4 = -4 \times 10^{-5}$ Å^4 denoting a slight asymmetry. The increase of the Sn-O coordination number at 0.05% with respect to the other diluted samples indicates a different morphology than that observed when clustering occurs; consider that the parameters reported in Table 1 are obtained without any constraint and confirmed both by the FEFF procedure and by direct comparison with the experimental phase and amplitude of the reference crystal. As the QD are embedded into an oxide network, the decrease of the Sn-O coordination number at 0.1 and 0.2% therefore should be attributed to a random distribution of the oxygen of the matrix not in ordered configuration at the border of the SnO_2 crystallites.

For the intermediate concentrations 0.1, 0.2, 0.3, and 0.5% we note a progressive increase of the coordination number with the increase of the concentration, reaching the value of the reference compound at 0.5%. This trend is verified for all the three shells reported in Table 1 demonstrating the formation of clusters [24–26]

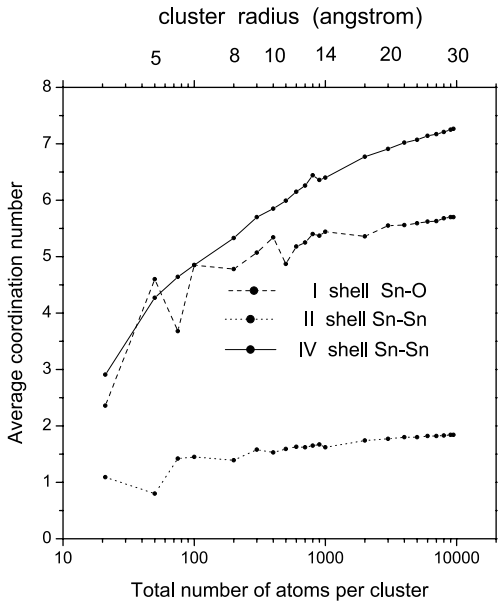

Fig. 5. Average coordination numbers for the first (Sn-O), second (Sn-Sn), and fourth (Sn-Sn) shells calculated for SnO_2 spherical clusters as a function of the size. The reduction with respect to the bulk value is due to the surface contribution. The reported dots correspond to the calculated values; note that the data have not a regular trend because, when the size increases, other atoms of the structure are added and therefore the average value can scatter, mainly for small sizes; of course the general trend should increase towards the bulk coordination values, respectively 6, 2, and 8. The line is a guide to the eye.

whose size is dependent on the concentration. In other terms, the modification of the coordination numbers can be simply explained if the precipitation of SnO_2 agglomerates of limited radius can give a surface contribution with coordination number reduced with respect to the internal one; the average value measured by the EXAFS technique, in fact, is a precise indication of the limited radius of these nanocrystals; therefore, at 0.5% as well as for higher concentrations the dimensions of the precipitates are quite large so to obtain the crystal parameters; at lower dilution, the regularity of the N value as a function of the concentration, not only for Sn-O but also for the two Sn-Sn higher shells, strongly supports we are dealing with an ensemble of quantum dots (QD) of reduced size; then, this size can be worked out just modifying the concentration of the semiconductor into the matrix. This conclusion can be corroborated by a simple check: in fact, in a spherical cluster of radius r there is a definite number of internal Sn atoms and of surface Sn atoms; whereas the internal atoms have the crystal coordination numbers, a surface shell atom has a reduced coordination as much as it is closer to the surface. As the geometrical distribution of atoms in the cluster is known, a simple geometrical exercise can exactly count the number of atoms in the coordination shell of each Sn atom in the cluster, calculating afterwards the average value. This calculation is reported in Figure 5 for the I, II and IV coordination shells, as a function of the cluster size. Comparing with the experimental

values, on the basis of the nice matching of all the coordination numbers, we can affirm that:

at 0.1% QD of 5 Å radius,
at 0.2 % QD of 10 Å radius,
at 0.3 % QD of 14 Å radius

were obtained. The above sizes, being evaluated by a simultaneous check of three coordination numbers, result with a quite small uncertainty, lower than 5%. We add some comments about the other parameters of Table 1; we observe that for smaller sizes the Sn-O distance is somewhat contracted whereas the DW factor results magnified; this behaviour is consistent with the size reduction considering that the surface bonds can undergo a contraction because of the breaking of the translational symmetry, particularly as concerns the first shell; for the same reason, the opposite applies to the vibrational amplitude expanded with respect to the crystal mainly at the smaller sizes.

It could be hypothesized that a mixture of SnO_6 and/or SnO_4 "molecules" could be mixed up with the clusters in the dilution range 0.1–0.3%; however, this hypothesis can be excluded for the following reasons:

i) this mixing, if present, would dramatically reduce the coordination of both second and fourth Sn-Sn coordination shell, at any dilution;

ii) the first Sn-O coordination, in the previous hypothesis, would be lower than that reported for 0.1 and 0.2% and this is not compatible with the correspondent Sn-Sn coordinations;

iii) at 0.3% the σ^2 value does not seem too much influenced by the higher value of the single molecules; we therefore conclude that a negligible, if any, presence of single molecules is present at any higher dilution.

The previous results compare with the data reported in reference [4] for indium oxide; in contrast however, we get here a regular dependence on the dilution which can be used for selecting the required average size of the confined QD, tailoring desired quantum optical transitions.

In conclusion we have demonstrated how to confine SnO_2 quantum dots in the nanosize range using a simple melting process with the proper concentration of the semiconductor into the glass matrix. Moreover, we have showed that in this matrix molecular confinement of distant noninteracting SnO_6 and SnO_4 can be uniformly obtained.

We wish to acknowledge the staff of GILDA and ESRF for the excellent assistance during the experiments. Thanks are due in particular to Stefano Colonna and Pierlorenzo Solari of the GILDA beamline, and to G. Malandrino for the diffraction analyses. We thank also Professor I. Pollini and Mr. D. Cipriani for the sample preparation.

References

1. Seok-Kyun Song, Phys. Rev. B **60**, 11137 (1999)
2. A. Diéguez, A. Romano-Rodríguez, J. Ramön Morante, N. Bârsan, U. Weimar, W. Göpel, Appl. Phys. Lett. **71**, 1957 (1997)
3. W.K. Man, H. Yan, S.P. Wong, I.H. Wilson, T.K.S. Wong, J. Vac. Sci. Tech. **14**, 1593 (1996)
4. G. Faraci, A.R. Pennisi, R. Puglisi, A. Balerna, I. Pollini, Phys. Rev. B **65**, 24101 (2002)
5. H. Kim, C.M. Gilmore, A. Piqué, J.S. Ilorwitz, H. Mattoussi, H. Murata, Z.H. Kafafi, D.B. Chrisey, J. Appl. Phys. **86**, 6451 (1999)
6. D.D. Edwards, T.O. Mason, F. Goutenoire, K.R. Poeppelmeier, Appl. Phys. Lett. **70**, 1706 (1997)
7. P. Serrini, V. Briois, M.C. Horrillo, A. Traverse, L. Manes, Thin Solid Films **304**, 113 (1997)
8. Di Liu, Prashant V. Kamat, J. Chem. Phys. **105**, 965 (1996)
9. K.C. Mishra, K.H. Johnson, P.C. Schmidt, Phys. Rev. B **51**, 13972 (1995)
10. J. Zuo, C. Xu, X. Liu, C. Wang, C. Wang, Y. Hu, T. Qian, J. Appl. Phys. **75**, 1835 (1994)
11. U. Woggon, *Optical Properties of Semiconductor Quantum Dots* (Springer-Verlag, Berlin, 1997)
12. F. Lawson, Nature **215**, 955 (1967)
13. R.W.G. Wyckoff, *Crystal structures* (Wiley, New York, 1964)
14. G. Faraci, A.R. Pennisi, A. Balerna, H. Pattyn, G.E.J. Koops, G. Zhang, Phys. Rev. Lett. **86**, 3566 (2001); G. Faraci, S. La Rosa, A.R. Pennisi, S. Mobilio, G. Tourillon, Phys. Rev. B **43**, 9962 (1991)
15. A. Pinto, A.R. Pennisi, G. Faraci, G. D'Agostino, S. Mobilio, F. Boscherini, Phys. Rev. B **51**, 5315 (1995); G. Faraci, S. La Rosa, A.R. Pennisi, S. Mobilio, I. Pollini, Phys. Rev. B **45**, 9357 (1992)
16. G. Faraci, A.R. Pennisi, J.L. Hazemann, Phys. Rev. B **56**, 12553 (1997); F. Zontone, F. D'Acapito, G. Faraci, A.R. Pennisi, Eur. Phys. J. B **19**, 501 (2001)
17. S. Pascarelli, F. D'Acapito, G. Antonioli, A. Balerna, F. Boscherini, R. Cimino, G. Dalba, P. Fornasini, G. Licheri, C. Meneghini, F. Rocca, S. Mobilio, ESRF Newslett. **23**, 17 (1995)
18. S. Pascarelli, F. Boscherini, F. D'Acapito, J. Hrdy, C. Meneghini, S. Mobilio, J. Synch. Rad. **3**, 147 (1996)
19. P.A. Lee, P.H. Citrin, P. Eisenberger, B. M. Kincaid, Rev. Mod. Phys. **53**, 769 (1981)
20. E.A. Stern, B.A. Bunker, S.M. Heald, Phys. Rev. B **21**, 5521 (1980)
21. J. Mustre de Leon, J.J. Rehr, S.I. Zabinsky, R.C. Albers, Phys. Rev. B **44**, 4146 (1991); J.J. Rehr, R.C. Albers, S.I. Zabinsky, Phys. Rev. Lett. **69**, 3397 (1992)
22. J.J. Rehr, S.I. Zabinsky, A. Ankudinov, R.C. Albers, Physica B **208-209**, 23 (1995); E.A. Stern, M. Newville, B. Ravel, Y. Yacoby: *ibid.* p. 117
23. This contribution can be enhanced using a $k^2\chi(k)$ curve which was also Fourier transformed; the best fit data were confirmed and the third shell with 4 O gave the following parameters: Sn-O distance 3.59 Å, $\sigma^2 = 0.0021$ Å^2; its relative yield with respect to the Sn-Sn fourth shell was 10%.
24. P.A. Montano, G.K. Shenoy, E.E. Alp, W. Schulze, J. Urban, Phys. Rev. Lett. **56**, 2076 (1986)
25. P.A. Montano, W. Schulze, B. Tesche, G.K. Shenoy, T.I. Morrison, Phys. Rev. B **30**, 672 (1984)
26. M.A. Marcus, M.P. Andrews, J. Zegenhagen, A.S. Bommannavar, P. Montano, Phys. Rev. B **42**, 3312 (1990)